ELSEVIER

International Journal of Mass Spectrometry 208 (2001) 205–225

International Journal of Mass Spectrometry

Ion discrimination during ion accumulation in a quadrupole interface external to a Fourier transform ion cyclotron resonance mass spectrometer

Mikhail E. Belov, Evgenii N. Nikolaev, Richard Harkewicz, Christophe D. Masselon, Kim Alving, Richard D. Smith*

Environmental Molecular Sciences Laboratory, Pacific Northwest National Laboratory, P.O. Box 999, Richland, WA 99352, USA

Received 23 October 2000; accepted 30 March 2001

Abstract

When coupled with high-performance capillary separations, Fourier transform ion cyclotron (FTICR) mass spectrometry provides powerful new capabilities for proteomic studies. Selective ion accumulation in a two-dimensional quadrupole device external to an FTICR mass spectrometer has been shown to increase its sensitivity, dynamic range, and duty cycle. In this article, we have evaluated the operation of a linear quadrupole ion trap coupled to a 3.5-tesla FTICR mass spectrometer in the presence of high space charge. On increasing the ion population in the linear quadrupole trap, pronounced *m/z* discrimination was observed. We have found that the superposition of the applied quadrupole rf and dc fields, the effective dc field from space charge within the quadrupole, and the quadrupole fringing fields at the quadrupole entrance and exit result in ion instability and *m/z* discrimination. After optimizing experimental parameters responsible for *m/z* discrimination, capillary LC-separated tryptic peptide ions (from a bovine serum albumin digest) were shown to be externally accumulated and detected using the FTICR mass spectrometer without evident *m/z* discrimination. (Int J Mass Spectrom 208 (2001) 205–225) © 2001 Elsevier Science B.V.

Keywords: Electrospray; FTICR-MS (Fourier transform ion cyclotron resonance mass spectrometry); Selective external ion accumulation; Ion discrimination; Ion stability

1. Introduction

When combined with high-performance capillary liquid chromatography (HPLC) or capillary isoelectric focusing (CIEF), Fourier transform ion cyclotron resonance mass spectrometry (FTICR-MS) provides a powerful new tool for proteomic studies [1,2]. In one highly promising approach, protein extracts or fractions are digested with trypsin and injected into a packed capillary column for subsequent separation. The separated tryptic peptides are then introduced on-line to an electrospray ionization (ESI) source of an FTICR mass spectrometer. The sensitivity, dynamic range, and duty cycle provided by FTICR has been shown to be increased by ion trapping and accumulation in a linear multipole trap positioned externally to an FTICR cell [3–5]. If extended accumulation periods can be used and ion transfer from the accumulation quadrupole to the FTICR cell and the

* Corresponding author. E-mail: dick.smith@pnl.gov

PII S1387-3806(01)00434-1

dynamic trapping [3] is efficient, significantly increased sensitivity can be achieved.

Accurate determination of the neutral masses for peptides and proteins is enhanced by resolution of the isotopic distributions and charge-state correlation as provided by FTICR [6]. However, it is important that ions be detected across the desired *m/z* range without significant bias. We have also shown recently that the automated calibration of FTICR mass spectra benefits significantly from the detection of several charge states for peptides ions [7]. In addition, if lower (or higher) mass-to-charge ratio (*m/z*) peptide ions were discriminated against during accumulation in the external trap, the information on the tryptic peptides eluting from a capillary column would be less complete. We have previously reported on efforts aimed at the development of generally useful methods for selective external ion accumulation in a quadrupole interface/ion guide of a FTICR mass spectrometer [4,8]. To prevent overfilling the external trap, higher-abundance ions can, after initial measurement, be preselected and ejected before external accumulation, thus trapping only lower-abundance species and, potentially, increasing overall dynamic range. However, a significant increase in the ion accumulation time, characterized by higher populations of lower-abundance ions in the external trap, can be accompanied with pronounced discrimination with respect to ion *m/z*. This problem is exacerbated by the higher ion currents provided by the use of an electrodynamic ion funnel in the ESI-FTICR interface [9], which can substantially negate additional efforts to enhance sensitivity by such approaches.

Significant progress in understanding *m/z* discrimination and distortion of the ion stability diagram in the presence of higher space charge has been made both theoretically and experimentally with three-dimensional quadrupolar ion traps [10–14]. The first region of the ion stability diagram has been found to be considerably distorted at lower rf and dc fields (in the close vicinity to the origin of the ion stability diagram), resulting in ion instability at lower *q* Mathieu values and shifts of the apex position [11,14]. A noticeable spatial separation of different *m/z* ions confined in onion-like layers has been reported [15]. This separation has been invoked to explain a significant variation in mass resolution when ejecting ions at different rf and dc fields.

Surprisingly, operation of linear (two-dimensional) ion traps in the presence of higher space charge has remained relatively unexplored. Senko et al. [3] have used an rf only octopole as an external linear ion trap for a FTICR mass spectrometer. Campbell et al. [16] have reported on a linear two-dimensional quadrupole ion trap coupled to an orthogonal linear time-of-flight mass spectrometer (TOF-MS). Parent ion fragmentation resulting from ion neutral collisions has been observed when resonantly ejecting peptide ions from the rf only quadrupole trap. Increasing ion population in the linear ion trap invariably pushes ions to regions of higher rf field, where ion heating and dissociation may occur. Similarly, pronounced dissociation has been observed after accumulation of large ion populations in an external linear hexapole trap of an FTICR mass spectrometer [17].

With increasing ion population in a linear trap, treatment of ion motion based on a single-ion approximation becomes invalid. A cloud of charged particles exhibits many of the collective phenomena associated with neutral plasmas. The criterion for describing a weakly correlated ensemble of charges as a plasma is based on comparing the cloud size to the Debye length, λ_D [18]

$$\lambda_D = \sqrt{\frac{\varepsilon_0 kT}{z^2 e^2 n}}. \quad (1)$$

Here, k is Boltzmann's constant, T is the temperature of the ions, n is the number density of charges, z is the ion charge, and e is the elementary charge.

In the case of a linear quadrupole trap, the maximum charge density is determined by the rf field and can be estimated in the zero-temperature approximation as [19,20]

$$n = \frac{4\varepsilon_0 V_{rf}^2}{m\omega_0^2 r_0^4}, \quad (2)$$

where ε_0 is the vacuum permittivity, V_{rf} is the peak-to-ground rf amplitude, m is the ion mass, ω_0 is the angular drive frequency of the quadrupole, and r_0

is the quadrupole inscribed radius. For singly charged bradykinin ions at $V_{rf} = 200$ V, $\omega_0 = 2\pi \times 600$ kHz, $r_0 = 4.1$ mm, the Debye length, λ_D is ~0.12 mm. We use peak-to-ground voltage when referring to V_{rf}. Given a sufficient ion current into the linear trap, the ion cloud will expand both axially and radially as it fills the trap volume. Under these conditions, the ion cloud in all its dimensions is considerably larger than the Debye length and should be treated as a nonneutral plasma [18,21].

In this article we report on the *m/z* discrimination observed at longer accumulation times in a external linear quadrupole trap of a 3.5-tesla FTICR mass spectrometer. The discrimination was studied as a function of a number of parameters, for example, ion accumulation time, trapping dc potentials, rf amplitude, and frequency, dc-axial field, and so forth. Possible mechanisms of ion ejection, as a result of superposition of, first, the rf field of the quadrupole and the dc field from the space charge generated by a trapped ion cloud and, second, the rf field and the fringing fields from trapping electrodes at the ends of the linear quadrupole, are presented and discussed.

2. Experimental

The FTICR mass spectrometer used in the experiments is based on instrumentation described previously [22,23]. The instrument uses a 3.5-tesla unshielded superconducting solenoid magnet (Oxford Instruments, UK). The mass spectrometer incorporates an ESI ion source with an ion funnel and a collisional focusing quadrupole, an external accumulation interface, an electrostatic ion guide and a cylindrical dual cell combination. An Odyssey data station (Finnigan, Corp. Madison, WI) controlled event timing and applied potentials during the experiment. The vacuum system comprises six stages of differential pumping that gradually decrease the pressure from atmospheric to the ultrahigh vacuum in the region of the FTICR trap. The ESI source and the external accumulation interface consist of the first four differentially pumped stages.

ESI emitter voltages of ~2 kV were applied to produce positive ions. The 0.75-mm-i.d., resistively heated stainless steel inlet capillary used for droplet desolvation was maintained at ~120 °C and typically biased at +200 to +300 V. The first stage of differential pumping, which incorporates the electrodynamic ion funnel, was evacuated by a 43-L/s roots pump (Leybold AG, Cologne, Germany) to ~1–3 torr. The ions transmitted through the funnel exit electrode to the following stage were collisionally focused in a 150-mm-long quadrupole ion guide (field radius of 4.1 mm, 9.525-mm rod diameter) operated in rf-only mode (typically 250 $V_{p\text{-}p}$ at 430 kHz) at a pressure of 0.23 torr (obtained using a 18-L/s mechanical pump; Leybold AG, Cologne, Germany). The dc-offset potentials of +15 to +20 V were typically applied to the collisional quadrupole rods to assist transmission of the ions through the 2-mm-i.d. conductance limit between the collisional quadrupole and external accumulation interface. The conductance limit was biased at +15 to +20 V. The external accumulation interface incorporating three quadrupoles (field radii of 4.1 mm, 9.525-mm rod diameter) is shown schematically in Figure 1. The assembly designed for collisional focusing, ion selection, and ion accumulation was mounted in an 8″-o.d., six-way vacuum cross (MDC, Hayward, CA) and operated at a pressure of 5×10^{-5} torr. Positioned at the interface input, a 150-mm-long quadrupole ion guide operated in an rf-only mode at an amplitude of 560 $V_{p\text{-}p}$ and a frequency of 2.1 MHz, supplied to the +11 V dc-biased quadrupole rods by a commercial rf drive (Extranuclear Labs, Pittsburgh, PA). The middle, 100-mm-long, analytical quality quadrupole of the assembly was used for ion selection (referred to as the selection quadrupole). This quadrupole was enclosed in a differentially pumped vacuum region that allowed for pressure adjustment in the range of 10^{-2} torr to 10^{-4} torr without affecting the base pressure in the rest of the interface. The rods and the 2-mm-i.d. input and output conductance limits of the selection quadrupole were biased to +8 V, +6 V, and −19 V, respectively. The selection quadrupole was driven by

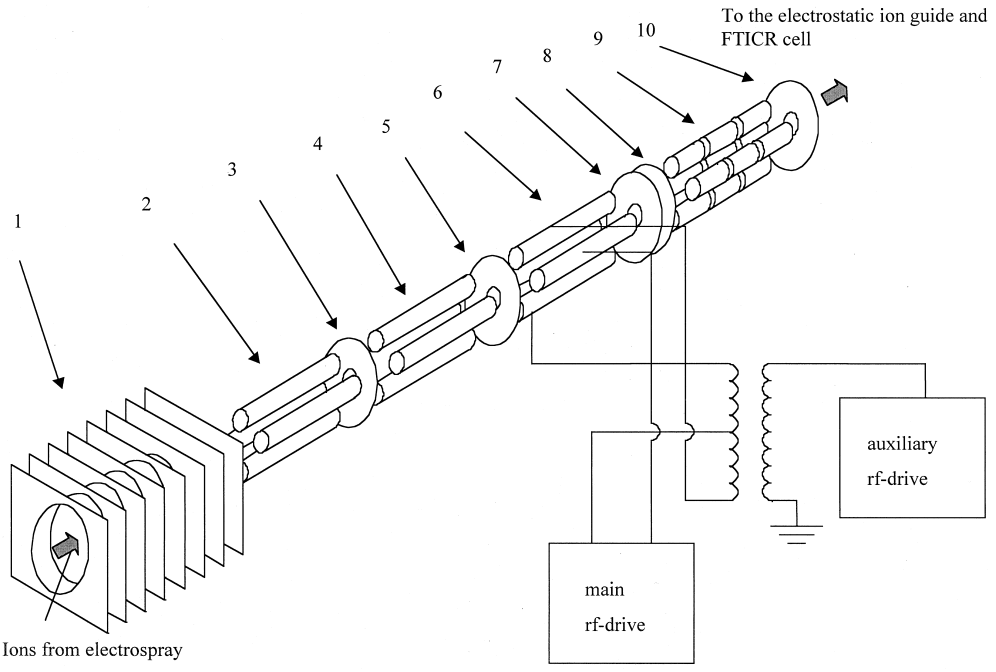

Fig. 1. A schematic diagram of the external accumulation interface with coupling of an auxiliary rf drive for dipolar excitation. 1 is the electrodynamic ion funnel, 2 is the collisional quadrupole, 3 is the conductance limit between the collisional and ion guiding quadrupoles, 4 is the ion guiding quadrupole, 5 is the entry plate of the selection quadrupole, 6 is the selection quadrupole, 7 is the exit plate of the selection quadrupole, 8 is the entry plate of the accumulation quadrupole, 9 is the accumulation quadrupole, and 10 is the exit plate of the accumulation quadrupole.

a built-in-house high-Q head controlled by a function generator (Model HP 33120A, Hewlett-Packard, Loveland, CO) and rf amplifier (Model 100A150A, Amplifier Research, Souderton, PA).

Two modes of ion selection were used based on, first, an rf/dc linear ramp and, second, rf-only selection using resonant dipolar excitation [16]. To implement the latter approach, two opposite rods of the selection quadrupole were coupled to the secondary coil of an auxiliary 1:1 transformer. The middle point of the transformer secondary coil was driven by the main rf drive at amplitudes of 300–1200 $V_{p\text{-}p}$ and frequencies ranging from 500 to 700 kHz. The excitation waveform was then applied to the primary coil of the transformer. The 10-cm-long exit quadrupole of the interface used for ion accumulation (referred to as the accumulation quadrupole) was segmented (each rod was segmented into 22 electrically isolated segments) to provide an axial electric field for prompt ion ejection. A built-in-house high-Q head drove the accumulation quadrupole at an rf amplitude of 220 $V_{p\text{-}p}$ and a frequency of 525 kHz. A linear electric field gradient of ~0.3 V/cm was applied along the accumulation quadrupole to create an axial potential well at the quadrupole exit. The rf voltage applied to the quadrupole segments was decoupled from dc and pulsed voltages generated by a built-in-house high-voltage multichannel amplifier through an RC circuit. The dc offset potentials of +12 V and −2 V were applied to the 4-mm-i.d. input and output conductance limits, respectively, of the accumulation quadrupole.

As external ion trapping increases the size of the ejected ion cloud compared with that of a continuous ion beam from the same source, we modified the previously described electrostatic ion guide in the high-vacuum region of the mass spectrometer [22].

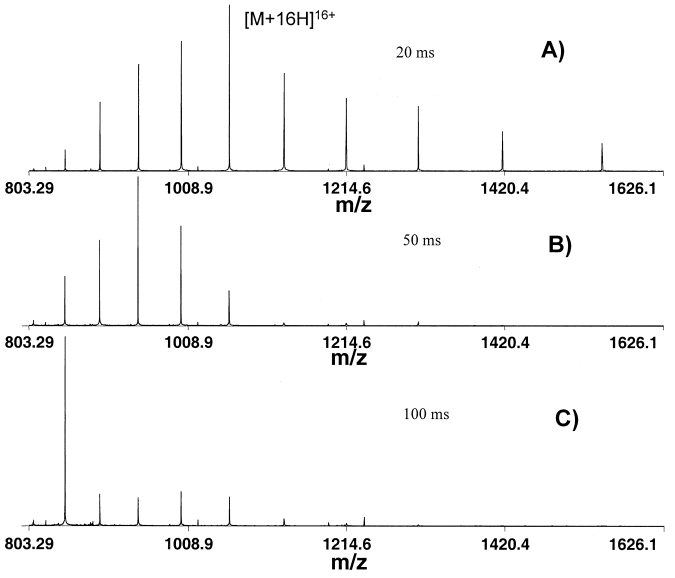

Fig. 2. The mass spectra of horse myoglobin ($\sim 10^{-6}$ M) at different accumulation times: (A) 20, (B) 50, and (C) 100 ms. The cooling time was 100 ms. The potentials at the accumulation quadrupole entry and exit plate were 17 and 30 V, respectively. $[M+20H]^{20+}$ and $[M+11H]^{11+}$ ions are characterized by q Mathieu value of 0.26 and 0.14, respectively.

Additional einzel lenses were added after the acceleration region. A pressure of 7×10^{-10} torr was maintained in the FTICR ion cell region.

The proteins and peptides were dissolved in a water:methanol:acetic acid solution (49:49:2 v%) at different concentrations ranging from 0.1 mg/mL to 2 pg/mL (the lowest concentration was $\sim 10^{-12}$ M for horse cytochrome *c*). The solutions were infused into the ESI source at a flow rate of 300 nL/min using a syringe pump (Harvard, South Natick, MA).

HPLC/FTICR-MS data sets were obtained using a capillary LC system based around a high-pressure syringe pump (ISCO, Inc, Lincoln, NE). The tryptic peptides were injected into a 150-μm i.d. $\times$ 60-cm-long capillary column packed with a 5-μm-diameter C_{18} separation medium (POROS 20R2, Perspective Biosystem, Framingham, MA). A solvent gradient was used to elute the peptides using 0.2% acetic acid in water (solvent A) and 0.2% acetic acid in 80% acetonitrile (solvent B). The peptides were eluted using a linear gradient of 0%–80% solvent B over 60 min. Solvents were delivered to the capillary column at a pressure of $\sim$6000 psi using two Isco model 100-DM pumps controlled by an Isco series D controller and an LC Packings Accurate microflow processor splitter (LC Packings, San Francisco, CA), resulting in a flow rate of ~ 1 μL/min.

3. Results

The effectiveness of ion accumulation in an external linear rf-quadrupole trap is affected by several parameters: first, accumulation and cooling times; second, a set of dc potentials supplied to the rods and entry and exit plates of the quadrupole and used to confine ions axially, and third, frequency and amplitude of the rf field, constraining ion motion in radial direction. The “ion accumulation” time corresponds to the time interval during which the rf potentials are applied to the collisional quadrupole rods. After trapping ions in the accumulation quadrupole, translational energy is damped by collisions with gas molecules before transfer to the FTICR cell. Reduced kinetic energy spreads provide higher efficiency for gated trapping. The time interval that trapped ions spend in the accumulation quadrupole after turning off the rf potential of the collisional quadrupole rods

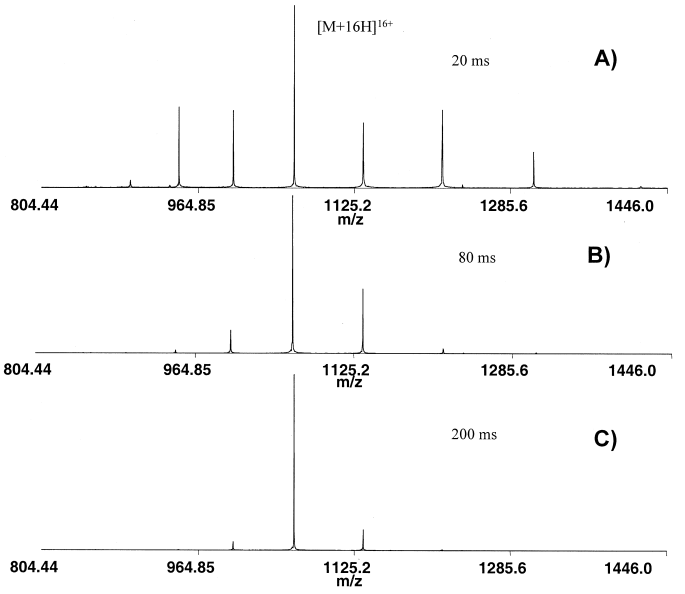

Fig. 3. The mass spectra of horse myoglobin ($\sim 10^{-6}$ M) at different accumulation times: (A) 20, (B) 80, and (C) 200 ms. The cooling time was 100 ms. The potentials at the accumulation quadrupole entry and exit plate were 18 and 21.5 V, respectively. $[M+16H]^{16+}$ ions has a q Mathieu value of 0.2.

(i.e., stopping further ion accumulation) will be referred to as the cooling time.

The patterns of *m/z* discrimination observed in this work were surprisingly complex. Fig. 2 shows the mass spectra of horse myoglobin ($\sim 10^{-6}$ M) obtained for different accumulation times. In this case, no axial electric field was used in the accumulation quadrupole, whose exit plate was biased to a potential of 30 V. A pronounced discrimination against lower charge states (at higher *m/z*) is observed on increasing the accumulation time. Fig. 3 shows the mass spectra of the same sample acquired at different accumulation times and a dc bias of 21.5 V at the exit plate of the accumulation quadrupole. The most abundant $[M+16H]^{16+}$ species dominates the spectrum at longer accumulation times. Fig. 4 shows the dependence of the ion signal of the most abundant charge states of horse myoglobin ($\sim 10^{-6}$ M) on the potential at the exit plate of the accumulation quadrupole. At trapping potentials corresponding to the ion's kinetic energy, sharp resonances are observed, leading to significant *m/z*-dependent discrimination during accumulation.

In the adiabatic approximation [24], the ion motion in an rf quadrupole is governed by the effective potential, V^* [25].

$$V^*(r) = \frac{z^2 e^2 V_{rf}{}^2 r^2}{m\omega_0{}^2 r_0{}^4}, \tag{3}$$

where r is the ion's radial coordinate within an ion cloud and the quadrupole fringing fields are neglected.

For lower ion populations in the rf-only quadrupole, the effective potential uniquely determines the efficiency of ion radial confinement, and a higher effective potential improves ion transmission. We found, on increasing the space charge in the quadrupole higher, that rf amplitudes at the same effective potential resulted in greater signal intensities.

The effective potential, V^*, for $[M+16H]^{16+}$ ions from myoglobin and the peak-to-peak amplitude of the rf field applied to the accumulation quadrupole as functions of the rf frequency are shown in Fig. 5(A). The dependence of the peak-to-peak amplitude on the drive frequency represents the resonance contour of

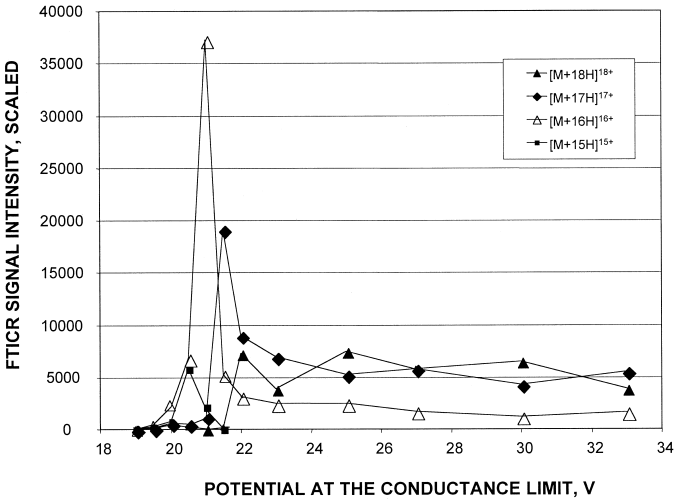

Fig. 4. The dependence of the signal intensities of $[M+15H]^{15+}$ to $[M+18H]^{18+}$ charge states of horse myoglobin ($\sim 10^{-6}$ M) on the potential at the accumulation quadrupole exit plate. The accumulation and cooling times were 200 and 50 ms, respectively.

the high-Q head used to drive the accumulation quadrupole. The increase in the effective potential at frequencies below 350 kHz is associated with the slower rate of the peak-to-peak amplitude decrease on decreasing the frequency. Figure 5(B) shows the effective potential of the accumulation quadrupole as a function of the rf amplitude applied to the accumulation quadrupole rods. The rf frequency was varied, whereas the input rf amplitude for the accumulation quadrupole high-Q head was maintained as constant (220 V peak to peak). On decreasing the rf frequency from 700 kHz, the effective potential initially increases, reaching a local maximum of ~5.3 V at an rf amplitude of ~230 V (corresponds to the high-Q head resonance at an rf frequency of ~600 kHz). Further decrease in the rf frequency is characterized by lower rf amplitudes (off-resonance) and lower effective potentials reaching a local minimum of ~1.5 V at an rf amplitude of ~80 V. For the same reason as in Fig. 5(A), the effective potential further increases on reducing the rf frequency below 350 kHz. Interestingly, the same effective potential is generated at different rf-amplitudes. For example, an effective potential of 3.5 V corresponds to rf amplitudes of ~60, ~170, and ~200 V (intersection points 3, 2, and 1 in Fig. 5B, respectively).

A detailed study of the accumulation quadrupole rf drive is required to understand the complex dependences of the ion signal at longer accumulation times. Further increase in the accumulation times (up to 300 ms) at higher trapping potentials resulted in discrimination against the lowest *m/z* ions. Fig. 6(A)–(C) shows the dependences of the ion signals for several charge states of horse myoglobin on the effective potential in the accumulation quadrupole at an accumulation time of 300 ms. It should be noted that, as the effective potential is *m/z* dependent, the intensities for the $[M+17H]^{17+}$, $[M+18H]^{18+}$, and $[M+19H]^{19+}$ ion signals are plotted against their own effective potentials in Fig. 6(A)–(C). The drive frequency was varied as a parameter. The dependences of the FTICR signal intensities on the effective potential were found to be three-branch parametric curves with three different signal intensities corresponding to a particular effective potential. The arrows indicate the direction of movement along the parametric curves on linearly decreasing the rf frequency. It should be pointed out that the signal intensity is a single-value function of the effective potential at lower ion populations in the quadrupole. Interestingly, at the same effective potential, higher signal intensities were observed at higher rf amplitudes. For example, the three different signal intensities for $[M+18]^{18+}$ myoglobin ions at an effective

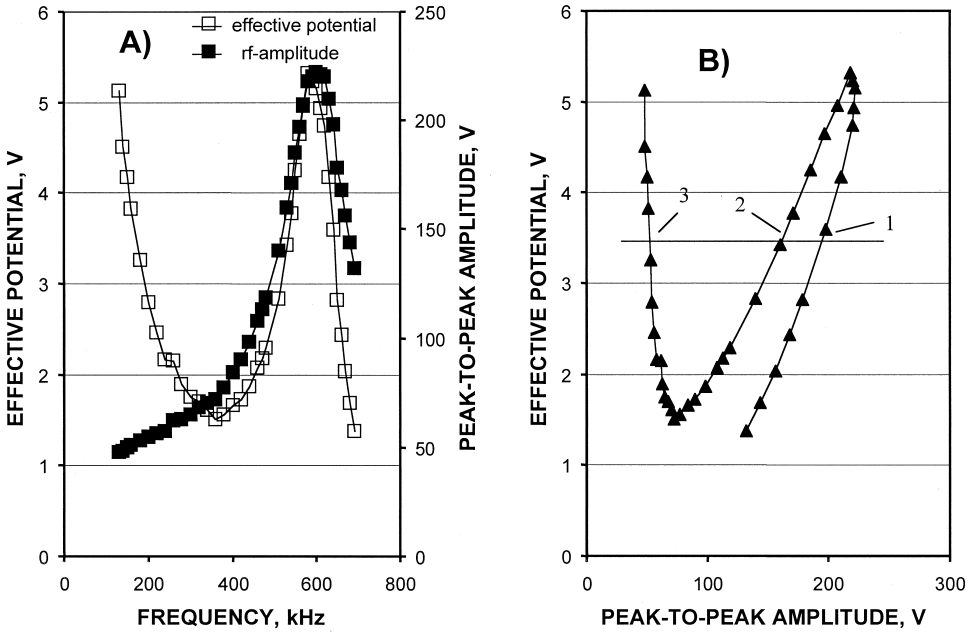

Fig. 5. (A) The effective potential and rf amplitude on the rods of the accumulation quadrupole as functions of the rf frequency. On the basis of the rf frequency and rf amplitude, the effective potential is derived using Eq. (3). (B) The dependence of the effective potential of the accumulation quadrupole on the rf amplitude on the rods of the accumulation quadrupole. The rf frequency was varied with the input rf amplitude to the accumulation quadrupole high-Q head maintained constant (~220 V peak to peak). Because of the high-Q head resonance at a frequency of ~600 kHz (see Fig. 5[A]), the same effective potential is generated at different rf amplitudes. For example, an effective potential of 3.5V is achieved at rf amplitudes of ~60, ~170, and ~200 V (points of 1, 2, and 3, respectively).

potential of 3.5 V (intersection points 1, 2, and 3) correspond to rf amplitudes of ~200, ~170, and ~60 V, respectively (points 1, 2, and 3 in Fig. 5[B]). The decrease in the quadrupole acceptance with decreasing rf frequency (i.e., higher *q* Mathieu) [26] (point 1 corresponds to higher rf frequency than that of point 3) can contribute to the decrease in signal intensities.

Fig. 7(A)–(D) shows the dependence of the horse myoglobin ion signal on the quadrupole drive frequency at an accumulation time of 500 ms. On decreasing the drive frequency from 625 to 590 kHz, the effective potential increases from 4.15 to 5.2 V, respectively (see Fig. 5A), increasing the accumulation quadrupole charge capacity. Therefore, greater space charge results in the shift of the isolated peak toward higher *m/z*.

Fig. 8(A) shows the mass spectrum of a mixture of bradykinin, gramicidin S, and angiotensin I at concentrations of 1.7×10^{-5} M, 1.6×10^{-5} M, and 2.3×10^{-5} M, respectively. The ions were trapped in the accumulation quadrupole after broadband accumulation for 300 ms (i.e., using nonselective ion accumulation). The singly charged species were found to be highly discriminated against, and pronounced fragmentation of doubly charged ions was also observed, presumably caused by rf-collisional heating. Fig. 8B shows that the mass spectrum of the same mixture of peptides accumulated for 300 ms in the segmented quadrupole after rf-only resonant ejection of doubly charged species in the selection quadrupole. Abundant singly charged ion peaks were detected with a significantly lower degree of fragmentation. Fig. 9(A)–(C), shows mass spectra of singly charged ions from the same peptide mixture at different accumulation times. The ions were nonselectively accumulated in the segmented quadrupole. In the

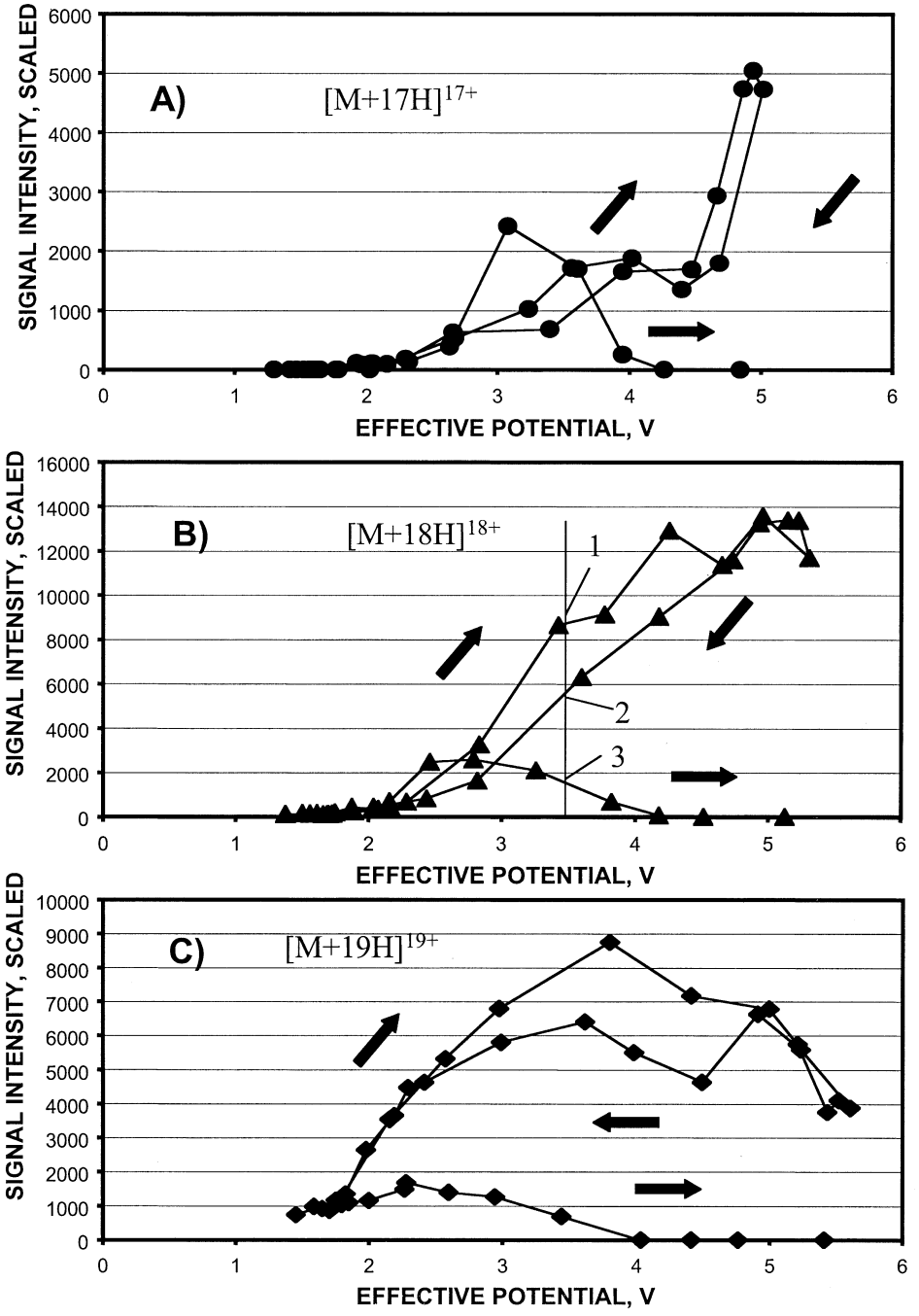

Fig. 6. The dependence of signal intensities of (A) $[M+17H]^{17+}$, (B) $[M+18H]^{18+}$, and (C) $[M+19H]^{19+}$ ions of horse myoglobin ($\sim 10^{-6}$ M) on the effective potential defined in Eq. (3). The arrows show the direction of movement along the parametric curves for linearly decreasing the rf frequency. The rf frequency is used as a parameter. The accumulation and cooling times were 300 and 50 ms, respectively. The potentials applied to the entry and exit plates of the accumulation quadrupole were 18 and 30 V, respectively. As the signal intensity versus the effective potential is a multivalue function, different signal intensities correspond to the same effective potential. For example, three different signal intensities (intersection points 1, 2, and 3 in Fig. 6[B]) correspond to an effective potential of 3.5 V. Comparing with Fig. 5(B) (see intersection points 1, 2, and 3 at an effective potential of 3.5 V) reveals that higher signal intensities are achieved at higher rf amplitudes for the same effective potential.

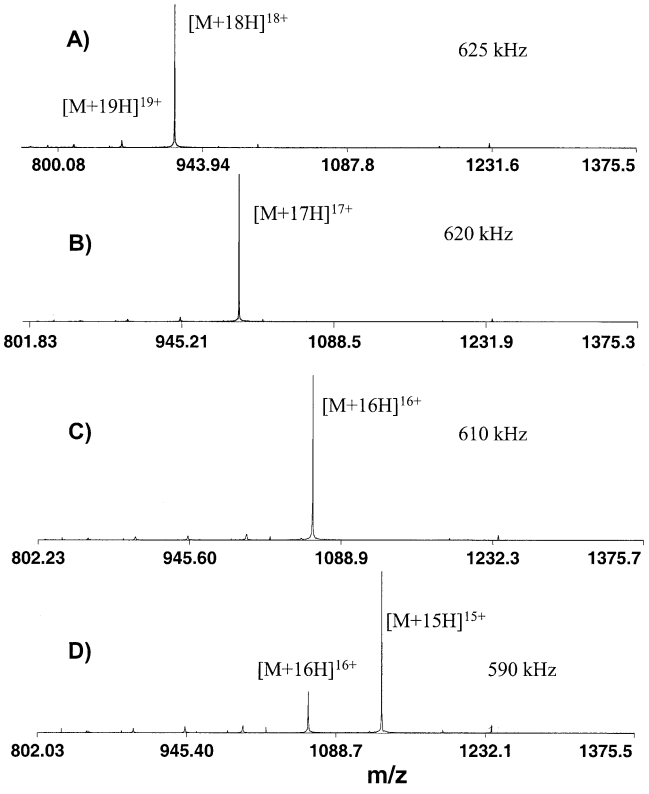

Fig. 7. Signal intensity of horse myoglobin ($\sim 10^{-6}$ M) as function of the quadrupole drive frequency. The accumulation and cooling times were 500 and 50 ms, respectively. $[M+18H]^{18+}$, $[M+17H]^{17+}$, $[M+16H]^{16+}$, and $[M+15H]^{15+}$ ions are characterized by q Mathieu parameters of (A) 0.192, (B) 0.185, (C) 0.180, and (D) 0.175, respectively.

presence of doubly charged ions, the intensities of higher *m/z* singly charged species (e.g., $[AnI+H]^+$) decrease at increased accumulation time. Fig. 10(A)–(C) shows mass spectra for singly charged species at different accumulation times after resonant ejection of doubly charge ions in the selection quadrupole. There is no significant discrimination observed against higher-*m/z* singly charged ions, and the intensities of all species increase on increasing the accumulation time.

Figure 11(A)–(D) shows the mass spectra of a polyethylene glycol (PEG 1000)/ultramark polymer mixture ($\sim 10^{-6}$ M) with a trace amount of horse myoglobin ($\sim 10^{-8}$ M) at different accumulation times. On increasing the accumulation time, we observed discrimination against heavier polymer ions (ultramark). A further increase in the accumulation time by an order of magnitude (up to 5 s) gave rise to the increase in signal intensities of ultramark ions and appearance of myoglobin ions. A subsequent fourfold increase in the accumulation time (up to 20 s) revealed strong discrimination against polymer ions and significant enhancement of myoglobin ion signal intensities.

Comparison of the mass spectra in Fig. 11(C)–(D) shows that on increasing the ion accumulation time, the myoglobin charge state distribution shifts toward higher *m/z*. Fig. 12 shows the mass spectra of horse myoglobin ($\sim 10^{-6}$ M) at different cooling times for an accumulation time of 20 ms. Significant discrimination against higher charge states is observed at longer cooling times, which we can ascribe to proton transfer processes.

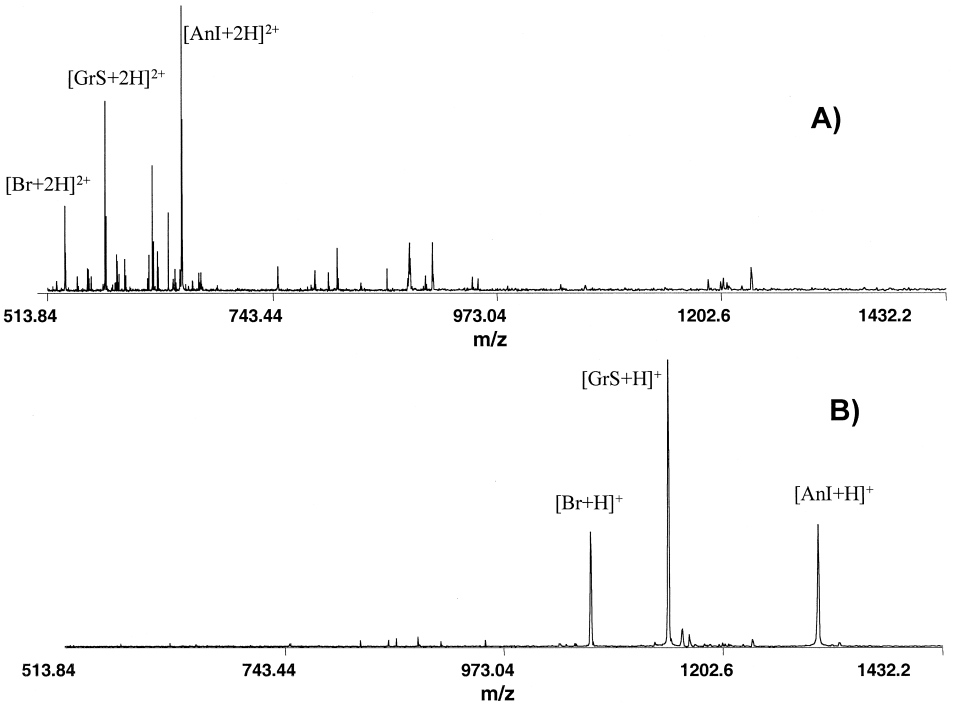

Fig. 8. The mass spectra of a mixture of bradykinin (Br), gramicidin S (GrS), and angiotensin I (AnI) acquired at an accumulation time of 300 ms and a cooling time of 50 ms. The potentials at the entry and exit plates were 18 and 30 V, respectively. (A) Broadband accumulation, (B) ion accumulation after ejecting all doubly charged species using rf-only dipolar excitation. $[Br+H]^+$, $[GrS+H]^+$, $[AnI+H]^+$, $[Br+2H]^{2+}$, $[GrS+2H]^{2+}$, and $[AnI+2H]^{2+}$ are characterized by q Mathieu parameters of 0.19, 0.18, 0.16, 0.38, 0.36, and 0.32, respectively.

4. Discussion

Because of the complexity of the observed *m/z* discrimination, we found it difficult to fit the experimental data to a general physical model. Presented below is our qualitative description and additional elucidation of some of the complex phenomena occuring in a linear quadrupole trap at higher ion populations.

4.1. Radial separation of trapped ions under steady state conditions in a zero-temperature approximation

At lower ion populations, ion motion is stable in an rf-only quadrupole if the stability parameter of Mathieu's equation, q, satisfies the relationship [24]:

$$q < 0.907; \tag{4}$$

$$q = \frac{4zeV_{rf}}{m\omega_0{}^2 r_0{}^2}. \tag{5}$$

If the frequency and amplitude of the rf field are chosen to meet the stability condition defined by inequality (3) and the change of the rf field over the full distance of oscillation is much smaller than the rf field itself (i.e., the adiabatic approximation is valid), the ion motion can be presented as a superposition of rapid oscillations and a smooth drift in the effective potential well, V^* [25] (see Eq. [3]). As follows from Eq. (3), the effective potential well is deeper for lower-*m/z* ions, implying stronger radial confinement.

As the effective potential is a quadratic function of the ion charge, whereas the Coulombic potential is linear proportional to the charge, one would expect radial separation of ions based on their *m/z*. Let us consider a particular point charge, *z*, located at the

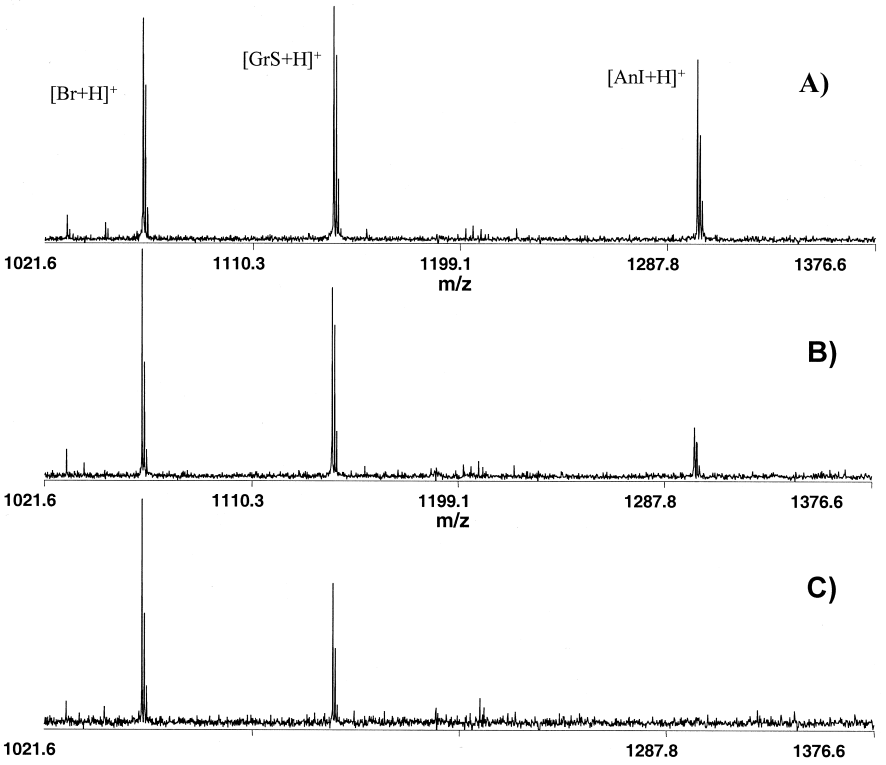

Fig. 9. The mass spectra of a mixture of bradykinin (Br), gramicidin S (GrS), and angiotensin I (AnI) acquired at different accumulation times and a cooling time of 50 ms. The potentials at the entry and exit plates were 18 and 30 V, respectively. The accumulation times during broadband accumulation were as follows: (A) 50, (B) 60, and (C) 70 ms. $[Br+H]^+$, $[GrS+H]^+$, and $[AnI+H]^+$ are characterized by q Mathieu values of 0.19, 0.18, and 0.16, respectively.

periphery of a cylindrically symmetric ion cloud having a linear charge density of Q. On the basis of the Gauss theorem, the space-charge-generated electric field at the position of the point charge, E_{SC} is

$$E_{SC} = \frac{Q}{2\pi\varepsilon_0 r_z}. \tag{6}$$

Under equilibrium conditions, one can assume that the Coulombic repulsion force is balanced by the effective potential force, F^* [20,26]:

$$F_{SC} = \nabla V^* = F^*; \tag{7}$$

$$\frac{Qze}{2\pi\varepsilon_0 r_z} = \frac{2z^2e^2{V_{rf}}^2 r_z}{m{\omega_0}^2{r_0}^4}. \tag{8}$$

Solving Eq. (8) with respect to r_z gives

$$r_z = K\sqrt{\frac{m}{z}}; \tag{9}$$

$$K = \sqrt{\frac{Q{\omega_0}^2{r_0}^4}{4\pi\varepsilon_0 e{V_{rf}}^2}}. \tag{10}$$

The above evaluation shows that under stationary equilibrium conditions lower-m/z ions are confined to smaller radii.

When a point charge $(z-1)$ is located at the periphery of an ion cloud formed by N_z ions, each having z charge, Eq. (8) will be modified as follows:

$$\frac{zN_z(z-1)e^2}{2\pi\varepsilon_0 r_{z-1}} = \frac{2(z-1)^2e^2{V_{rf}}^2 r_{z-1}}{m{\omega_0}^2{r_0}^4}. \tag{11}$$

Solving Eq. (11) with respect to r_{z-1} and taking into account Eq. (2) gives

$$r_{z-1} = \sqrt{\frac{z}{\pi(z-1)}\frac{m\omega_0^2 r_0^4}{4\varepsilon_0 V_{rf}^2}} = \sqrt{\frac{z}{(z-1)\pi n}} = r_{z\,max}\sqrt{\frac{z}{z-1}} \quad (12)$$

because $\sqrt{z/(z-1)} > 1$, $r_{z-1} > r_{z\,max}$. This indicates that higher-*m/z* ions can have motions influenced by the effective potential force outside of an ion cloud formed by lower-*m/z* ions.

After introducing additional $(z-1)$ charges to the system, the equation of balance of Coulombic repulsion and the effective potential force is governed by

$$\frac{zN_z(z-1)e^2 + (z-1)^2e^2\int_{r_{z-1\,min}}^{r_{z-1}} n_{z-1}(r_{z-1})2\pi r_{z-1}dr_{z-1}}{2\pi\varepsilon_0 r_{z-1}} = \frac{2(z-1)^2e^2V_{rf}^2 r_{z-1}}{m\omega_0^2 r_0^4}. \quad (13)$$

Differentiating Eq. (13) over r_{z-1} results in

$$n_{z-1} = \frac{4\varepsilon_0 V_{rf}^2}{m\omega_0^2 r_0^4}. \quad (14)$$

Comparing this with Eq. (2) and taking into account Eq. (12) shows that ions having $(z-1)$ charges will tend to form a concentric shell outside of the shell formed by z charge species and to have the same charge density. Radial separation of different *m/z* species will be further referred to as *m/z* stratification. Therefore, under steady state conditions in the zero-temperature approximation, one should have stratification of different *m/z* ions in spatially separated concentric shells of the same charge density. Though increases in temperature and ion-neutral collisions would inevitably smear the stratification pattern, lower-*m/z* ions are expected to be focused at smaller radii after cooling the ion cloud. Generalization of ion radial stratification for higher-order rf-only multipoles (e.g., hexapole, octopole, and stacked ring assembly) has recently been reported by Tolmachev et al. [27]. Direct modeling of ion motion in the accumulation quadrupole is also consistent with rough analytical estimates of ion radial separation [28].

4.2. Distortion of the ion stability diagram for an rf-only quadrupole at higher space charge

Let us estimate the distortion of the ion stability diagram caused by the space charge in the zero-temperature approximation. The electric-field strength inside a cylindrically symmetric ion cloud can be found based on Gauss's theorem:

$$\oint E_{SC}dS = \frac{\iint_{r,L} 2\pi r n dr dL}{\varepsilon_0}. \quad (15)$$

Here, $dS = 2\pi dr dL$ is the infinitely small surface area of an imaginary cylinder filled with charged species, n is the charge density defined in Eq. (2), and dL is the infinitely small length of the imaginary cylinder. Because of cylindrical symmetry, E_{SC} = const at a given r, and Eq. (15) can be solved with respect to E_{SC} as follows:

$$E_{SC}(r) = \frac{nr}{2\varepsilon_0} = \frac{2V_{rf}^2 r}{m\omega^2 r_0^4}. \quad (16)$$

Integrating Eq. (16) converts the space-charge-generated electric field, E_{SC}, to the potential φ_{SC}:

$$\varphi_{SC} = -\frac{V_{rf}^2 r^2}{m\omega^2 r_0^4} = -\frac{V_{rf}^2}{m\omega^2 r_0^4}(x^2 + y^2). \quad (17)$$

It is known from the theory of quadrupole mass filters that if the dc potential, U_{DC}, is applied to the quadrupole rods, the dc field inside the quadrupole is governed by the relationship [29].

$$\varphi_{DC} = \frac{U_{DC}}{r_0^2}(x^2 - y^2). \quad (18)$$

Comparing Eqs. (17) and (18), one can introduce an effective dc potential in the quadrupole, U_{DC}*, generated by the space charge:

$$\varphi_{SC} = \frac{U_{DC}^*}{r_0^2}(x^2 + y^2); \quad (19)$$

$$U_{DC}^* = -\frac{V_{rf}^2}{m\omega^2 r_0^2}. \quad (20)$$

In the presence of the dc field and for lower ion populations, the ion-stability diagram of a quadrupole is two-dimensional, with Mathieu's parameter, a_x given by [14,29].

$$a_x = \frac{8zeU_{DC}}{m\omega_0^2 r_0^2}. \quad (21)$$

By substituting U_{DC}* for U_{DC} in Eq. (21) and taking into account Eq. (5), the relationship between a_x and q_x ($q_x = q$) is

$$a_x = -q_x^2/2. \quad (22)$$

Therefore, in the presence of the space charge, Mathieu's equations for an rf-only quadrupole are similar to that for an rf/dc quadrupole except for the signs for a_x, a_y terms (i.e., space charge components, $a_x = a_y$), which are positive in both equations, as follows:

$$\frac{d^2x}{d\xi^2} + (k_{SC}a_x - 2q_x \cos 2\xi)x = 0; \quad (23)$$

$$\frac{d^2y}{d\xi^2} + (k_{SC}a_y + 2q_y \cos 2\xi)y = 0, \quad (24)$$

where $\xi = (\omega_0 t)/2$, $0 < k_{SC} < 1$, and a_x is determined by Eq. (22). The parameter k_{SC} is introduced into the Mathieu equation to account for space charge levels smaller than that predicted by Eq. (2) (e.g., because of ion losses in the fringing fields; an axial well depth that is less than the effective potential well resulting in axial ion losses; etc.).

Eqs. (23) and (24) were solved numerically, and the ion stability region as a function of q_x for k_{SC} ranging from 0 to 1 is shown in Fig. 13. For example, the ion motion in the quadrupole is stable for $0 < q_x < 0.8$ at the space charge density of 40% of its maximum ($k_{SC} = 0.4$). On increasing space charge (i.e., higher values of k_{SC}), the right boundary of the ion stability diagram, corresponding to lower-*m/z* ions, shifts to lower q_x. As compared with the inequality (4), applicable at lower ion densities in the quadrupole, greater space charge narrows the first stability region, that is, on increasing ion population in the quadrupole, lower rf amplitudes give rise to instability and ejection of lowest *m/z* ions from the quadrupole.

In the zero-temperature approximation, the maximum number density and the rf amplitude are closely bound (see Eq. [2]). Increasing the rf potential on the accumulation quadrupole rods (i.e., increasing the effective potential well depth) increases the maximum number of ions that can potentially be trapped in the quadrupole. However, increasing the number of ions in the quadrupole results in the instability and ejection of lower-*m/z* ions (see Fig. 13). Therefore, a trapped ion cloud rearranges itself in response to adding more ions by ejecting lower-*m/z* ions because of ion instability and higher-*m/z* ions because of radial ion stratification (e.g., see Fig. 3[C]).

4.3. Comparison of the models of ion radial stratification and ion instability with experimental data

Let us consider these models of ion radial stratification and distortion of the ion stability diagram in the context of the experimental data. Though discrimination in favor of lowest-*m/z* ions with increasing ion accumulation time (see Fig. 2) appears to be consistent with a radial ion stratification process, biased accumulation of higher-*m/z* ions (e.g., the isolation of the most abundant peak of $[M+16H]^{16+}$ ions [see Fig. 3] at longer accumulation times) needs further explanation.

It should be noted that during ion accumulation, the kinetic energy of ions entering the accumulation quadrupole is substantially determined by the potential (+20 V) applied to the conductance limit between

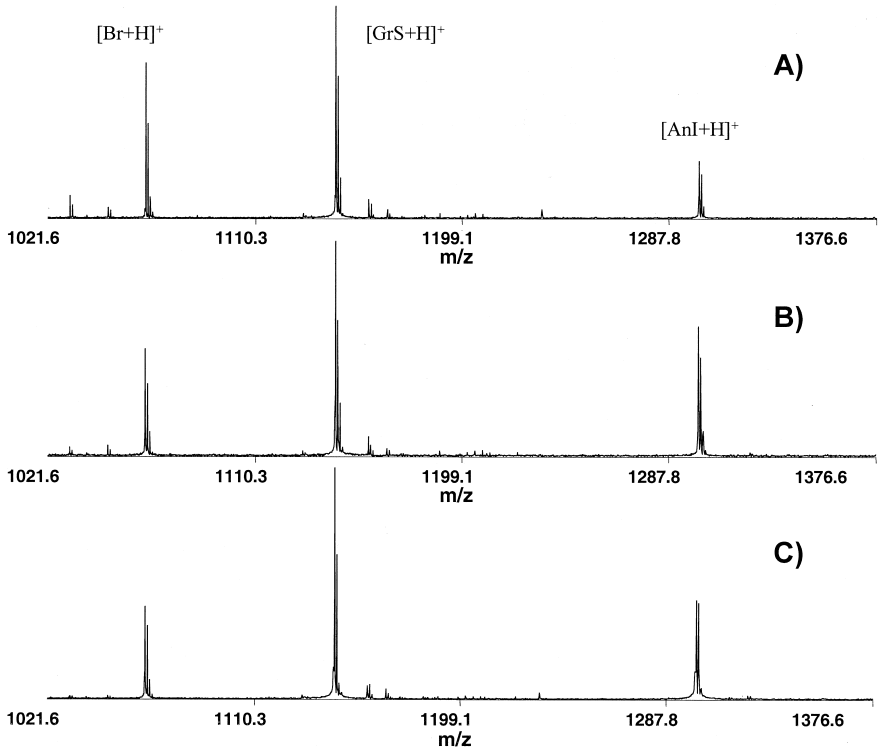

Fig. 10. The mass spectra of a mixture of bradykinin (Br), gramicidin S (GrS), and angiotensin I (AnI) acquired at different accumulation times and a cooling time of 50 ms. The potentials at the entry and exit plates were 18 and 30 V, respectively. The doubly charged species were ejected in the selection quadrupole using rf-only dipolar excitation. The accumulation times were as follows: (A) 60, (B) 100, and (C) 300 ms. $[Br+H]^+$, $[GrS+H]^+$, and $[AnI+H]^+$ are characterized by q Mathieu values of 0.19, 0.18, and 0.16, respectively.

the collisional and ion guiding quadrupoles. On decreasing the potential at the exit plate of the accumulation quadrupole, the ions penetrate deeper into the fringing electric field between the quadrupole rods and the exit plate. At longer accumulation times, a trapped ion cloud expands both radially and axially because of Coulombic repulsion and the space charge in the regions of the fringing field causes additional field perturbations. The fringing fields between the quadrupole rods and the exit plate, comprising an *m/z*-dependent component caused by the effective potential and an *m/z*-independent term from the electrostatic field, form a defocusing ion lens that affects ions during every second passage across the accumulation quadrupole (on average, it is estimated that myoglobin ions need ~80 passages across the accumulation quadrupole for collisional relaxation). Therefore, when the trapping potentials match the ion's kinetic energy, one would expect strong ion defocusing during trapping that could be *m/z* selective. The fringing field has been reported [30,31] to penetrate about two inscribed radii into a linear quadrupole. On increasing the dc potential at the quadrupole exit plate, the dc field penetrates deeper into the accumulation quadrupole, thus reducing the defocusing effect. We suspect that, along with ion radial stratification and ion instability, the space charge perturbation to the quadrupole fringing field is a contributing factor to the selective accumulation bias experimentally observed (see Figs. 3–4).

Similar discrimination effects were also observed for higher trapping potentials at the accumulation quadrupole exit plate (+30 V), longer accumulation times (0.5–2 s), and large entry total ion currents of

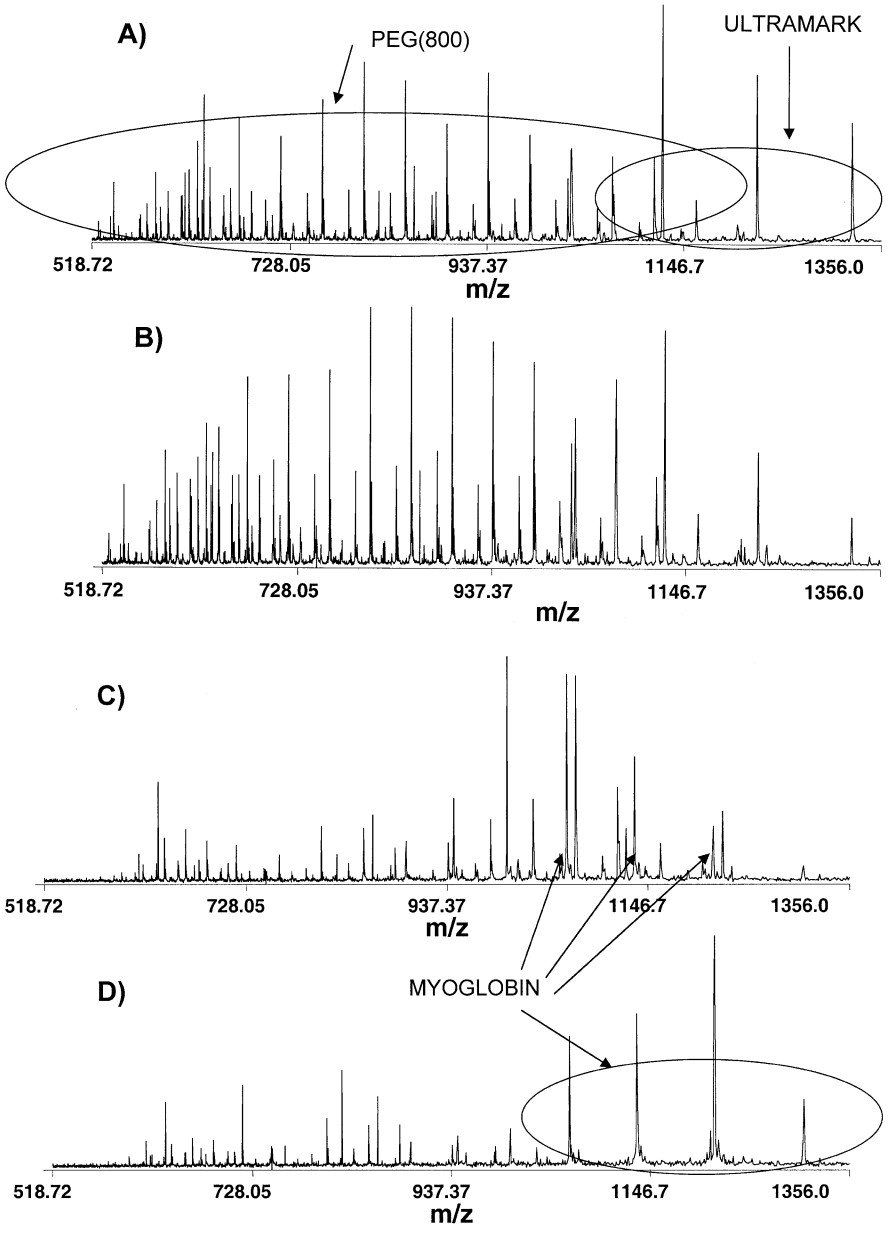

Fig. 11. The mass spectra of a mixture of polyethelene glycol (PEG 1000, $\sim 10^{-6}$M), ultramark ($\sim 10^{-6}$ M), and horse myoglobin ($\sim 10^{-8}$ M) acquired at different accumulation times and a cooling time of 50 ms. The accumulation time was (A) 200 ms, (B) 500 ms, (C) 2 s, and (D) 20 s. The *q* Mathieu value ranges from 0.17 ($[M+14H]^{14+}$ ion of horse myoglobin) to 0.4 (PEG ion peak at *m/z* 519.2).

1–2 nA. Both ion radial stratification and ion instability appear to contribute to isolation of the most abundant protein peaks in the middle of the charge-state distribution. While radial stratification radially "pushes" higher-*m/z* ions out of the quadrupole, the lowest-*m/z* ions experience the aforementioned space-charge-caused ion instability. These effects are postulated to result in the bias toward accumulation of *m/z* peaks in the middle of the charge-state distribution.

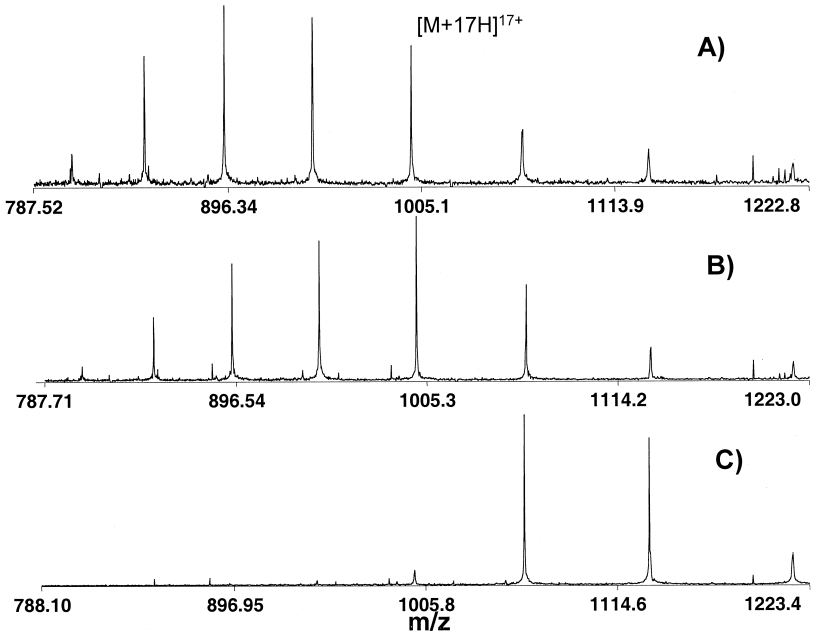

Fig. 12. The mass spectra of horse myoglobin ($\sim 10^{-6}$ M) at an accumulation time of 20 ms and different cooling times. The cooling time was (A) 200 ms, (B) 1 s, and (C) 10 s. The q Mathieu value is in the same range as in Fig. 2.

The estimate of distortion of the ion stability diagram for an rf-only quadrupole at higher space charge appears to be in accord with the experimental data shown in Fig. 6. The effective potential is converted to Mathieu's parameter, q, as follows:

$$q = \frac{4V^*}{V_{rf}}. \tag{25}$$

For example, an effective potential of ~5 V for $[M+18H]^{18+}$ myoglobin ions generated at a peak-to-peak rf amplitude of 210 V (see Fig. 6[A]) corresponds to $q \sim 0.2$. The detectable signal was observed up to $q \sim 0.5$ (Fig. 6[A]–[B]). Therefore, the first region of the ion stability diagram is narrowed to $q < 0.5$ in the presence of higher space charge. As follows from our analysis of the space-charge distorted-ion stability diagram (see Fig. 13), the stability region shrinks to $q < 0.7$ on reaching the maximum charge density, consistent with the experimental results.

We have previously reported [8] that during resonant rf-only dipolar excitation in some cases, higher rf amplitudes were required for ejection with longer accumulation times. This was attributed to the increased efficiency of ion–ion interactions within a dense ion cloud. Based on such nonneutral plasma "coupling" [32], one can suggest that the effective potential distribution distorts to "match" the strongly coupled ion cloud and that higher rf amplitudes result in higher ion populations in the quadrupole. This may account for the higher observed signal intensities corresponding to higher rf amplitudes at the same effective potential (see Fig. 6[A]–[C]).

The shift of the isolated charge state of horse myoglobin toward higher *m/z* on decreasing the quadrupole drive frequency (see Fig. 7[A]–[D]) appears to be qualitatively consistent with such a distortion of the ion stability diagram (see Fig. 13). As mentioned earlier, decreasing the quadrupole drive frequency from 625 to 590 kHz increased the effective potential from 4.15 to 5.2 V. This means that more ions can be trapped (higher k_{sc} in Fig. 13) on decreasing the frequency. Increasing the space charge narrows the ion stability diagram ($q_{max} \sim 0.68$ at the maximum

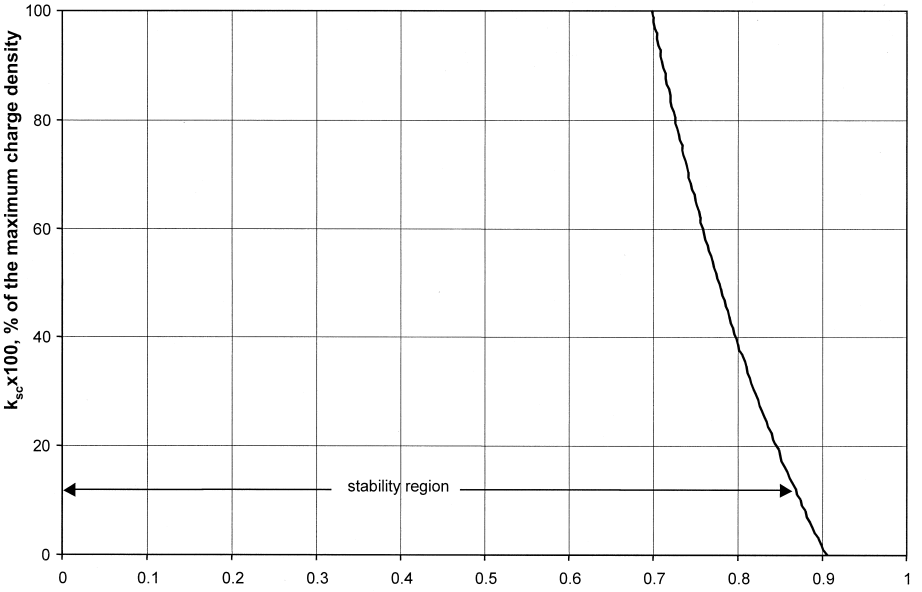

Fig. 13. Distortion of the ion stability diagram on increasing the space charge in an rf-only quadrupole. $k_{sc} \times 100$ is the percentage of the maximum charge density (see Eq. [2]), and q is Mathieu's parameter (see Eq. [5])

space charge density, compared with $q_{max} = 0.907$ in single-ion approximation), resulting in ejection of lower-*m/z* ions because of this space-charge-assisted ion instability.

The simple electrostatic model of *m/z* stratification developed in Eqs. (3)–(14) can be invoked to qualitatively explain the results for the peptide mixture. In the presence of both singly and doubly charged ions, the model predicts strong radial separation of different charge states, consistent with experiment (see Figs. 8[A], 9[A]–[C]). However, on ejecting the doubly charged species, there should still exist radial separation of different *m/z* species according to the model. No *m/z* discrimination was observed while accumulating singly charged ions in the quadrupole (see Figs. 10[A]–[C]). Apart from electrostatic interactions, ion-neutral collisions play a significant role in establishing the effective steady state condition of the ion cloud during accumulation. When entering the accumulation interface from the higher-pressure collisional quadrupole, lighter ions, whose trajectories are more susceptible to collisions with neutral particles, would necessarily expand to larger radii. Thus, ion-neutral interactions can counterbalance the *m/z* stratification effect over a narrower *m/z* range, resulting in the accumulation of singly charged peptide ions.

Though discrimination in favor of lighter PEG ions is consistent with radial *m/z* stratification (see Figs. 11[A]–[B]), the intensity increase for higher-*m/z* myoglobin ions (see Figs. 11[C]–[D]) at longer accumulation times (5–20 s) cannot be explained within the framework of this model. If myoglobin ions were radially positioned at the periphery of the ion cloud, the collisional effects would not result in the observed discrimination. Indeed, taking into account the concentrations of myoglobin and polymer species, the rate of diffusion losses of polymer ions would be expected to be two orders of magnitude greater than that of myoglobin ions. As the decrease in the diffusion rate on increasing the ion mass should be approximately linear [33], such a difference in diffusion losses is unlikely. It would be reasonable, then, to suggest that because of gas dynamic focusing, the myoglobin ions enter the accumulation quadrupole with smaller radial dispersion compared with that of the polymer ions. In other words, the myoglobin ions are initially introduced and distributed along the quadrupole axis and, because of cylindrical symmetry

of the ion cloud, the electrostatic repulsive forces from other species are cancelled out. The lower diffusion rates of myoglobin ions and their location within the ion cloud (which is characterized by reduced Coulombic repulsion from lower-*m/z* species) are believed to result in discrimination in favor of myoglobin ions at longer accumulation times.

Another type of discrimination was observed on increasing the cooling time in the accumulation quadrupole (see Fig. 12). It should be pointed out that this discrimination occurs for the number of ions in the accumulation quadrupole that is low enough to account for *m/z* stratification. The most probable explanation is that the number of ion-neutral collisions increases on increasing the cooling time, thus enhancing the probability of a proton transfer process. Multiply charged ions are more susceptible to collisional activation and would be expected to show greater losses caused by proton transfer at longer cooling times.

To summarize regarding the mechanisms causing discrimination, we believe that there are two major factors that contribute: ion radial stratification and ion instability caused by higher levels of space charge. As the number of ions trapped in the accumulation quadrupole contributes to the sensitivity and dynamic range of an FTICR instrument (i.e., larger ion populations in the accumulation quadrupole are expected to yield higher sensitivity and dynamic range), both ion radial stratification and space-charge-caused ion instability are undesirable effects limiting the potential of external ion accumulation. We are currently investigating several approaches aimed at disrupting radial stratification and increasing the space-charge capacity of the accumulation interface.

Ion perturbations in the accumulation quadrupole caused by fringing fields experienced during accumulation and proton transfer effects appear to be more readily minimized by increasing the potential applied to rear trapping plate of the accumulation quadrupole and by shortening the duration of ion cooling (where trapped ions are kept in the quadrupole without introducing new ions from the ESI source), respectively.

To minimize discrimination during external ion accumulation in a linear quadrupole ion trap, several conditions should be met. First, the potentials applied to the quadrupole trapping plates should exceed the ion kinetic energy by a few volts to minimize ion defocusing in the fringing rf and dc fields. Second, the accumulation time must be sufficiently short, or the ion current sufficiently small, to limit the ion population in the quadrupole. Sufficiently short accumulation time implies a trade-off between an achievable sensitivity/dynamic range and the mass spectrum quality (i.e., absence of discrimination). Increasing the charge density in the quadrupole up to its capacity results in *m/z* stratification and ion instability caused by the space charge and, thus, *m/z* discrimination. Third, the ion cooling time should be chosen to minimize the ion's kinetic energy spread and the probability of proton transfer process caused by ion-neutral collisions.

Following this strategy, 256 K data sets were acquired for capillary LC-FTICR analyses. Fig. 14 shows a reconstructed TIC chromatogram for a separation of a tryptic digest of a 0.01-mg/mL solution of bovine serum albumin. An accumulation time of 3 s was experimentally found to maximize signal intensity with no *m/z* discrimination observed. Longer accumulation times ($>$5 s) led to pronounced discrimination effects. Under optimized experimental conditions, 4180 different isotopic distributions (singly and doubly charged ions) were detected.

It should be noted that to increase signal intensities of less abundant species during LC-FTICR experiment, the ion accumulation time needs to be increased, a step that would result in *m/z* discrimination during portions of the analysis. To avoid such discrimination, the higher abundant species could ideally be identified and filtered out while passing through the selection quadrupole in the course of the separation, providing the basis for significant dynamic range expansion. As abundant species are typically dispersed across the mass spectrum, rf-only resonant dipolar excitation tuned to eject particular *m/z* ions at a mass resolution of 30–50 [4,8] should be highly effective for this purpose. An approach for enhancing the intensities of less abundant species during capillary LC-FTICR without *m/z* discrimination would

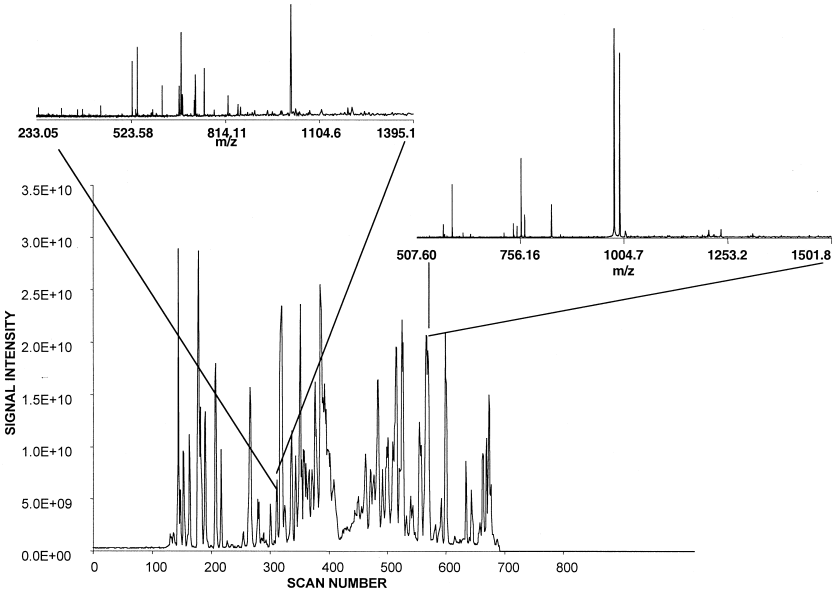

Fig. 14. The total ion current chromatogram of bovine serum albumin digest at a concentration of 0.01 mg/mL. Accumulation and cooling times were 3 s and 300 ms, respectively. The potential applied to the rear trapping plate of the accumulation quadrupole was 30 V. The insets represent the mass spectra acquired during individual scans.

involve, first, identifying the mass-to-charge ratio(s) of the most abundant species using broadband accumulation and, second, converting the identified *m/z*'s to a set of excitation frequencies that are applied for ejecting the most abundant species in the acquisition that immediately follows. The result is a methodology for effective dynamic range expansion that includes the advantages of external accumulation. We have already implemented this data-dependent approach for mixtures of peptides and proteins and are currently evaluating it for characterization of whole-proteomic digests, which will be the subject of future publications.

5. Conclusions

A selective ion accumulation capability in a triple quadrupole arrangement interfaced "external" to an FTICR mass spectrometer has been successfully implemented. On increasing the ion accumulation time in the accumulation quadrupole, pronounced and complex *m/z* discrimination effects were observed. The discrimination effects were studied experimentally and by computer modeling to provide a qualitative explanation for the experimental results. It was established that combination of the quadrupole rf field, the space-charge-generated dc field from the trapped ion cloud, and fringing fields from the quadrupole-trapping electrodes are the major factors leading to *m/z* discrimination effects. At decreased ion accumulation and cooling times, and increased trapping potentials during external ion accumulation in the segmented quadrupole, unbiased accumulation was achieved. Selective *m/z* accumulation, where such discrimination is avoided, promises to greatly enhance the dynamic range achievable in FTICR.

Acknowledgements

We are grateful to Drs. Mikhail Govshkov, Ljiljana Pasa-Tolic, Sergey Rakov, Aleksey Tolmachev, and A.A. Vedenov for helpful discussions. Portions of this research were supported by the National Institutes of Health National Center for Research Resources, grant

RR 12365, and the National Cancer Institute under Grant CA86340. The ESI-FTICR instrumentation design and construction was supported as part of the development of the Environmental. Molecular Sciences Laboratory at Pacific Northwest National Laboratory (PNNL) by the office of Biological and Environmental Research, U.S. Department of Energy. PNNL is a multiprogram national laboratory operated by Battelle Memorial Institute for the U.S. Department of Energy under Contract DE-AC06-76RLO 1830. E.N. Nikolaev acknowledges the partial support of this research by the Russian Foundation for Basic Research (grants 99-03-332663 and 99-04-49261).

References

[1] P.K. Jensen, L. Pasa-Tolic, G.A. Anderson, J.A. Horner, M.S. Lipton, J.E. Bruce, R.D. Smith, Anal. Chem. 71 (1999) 2076.
[2] T.D. Veenstra, S. Martinovic, G.A. Anderson, L. Pasa-Tolic, R.D. Smith, J. Am. Soc. Mass Spectrom. 11 (2000) 78.
[3] M.W. Senko, C.L. Hendrickson, M.R. Emmett, S.D.-H. Shi, A.G. Marshall, J. Am. Soc. Mass Spectrom. 8 (1997) 970.
[4] M.E. Belov, E.N. Nikolaev, G.A. Anderson, H.R. Udseth, T.P. Conrads, T.D. Veenstra, C.D. Masselon, M.V. Gorshkov, R.D. Smith, Anal. Chem. 73 (2001) 253.
[5] Y. Wang, S.D.-H. Shi, C.L. Hendrickson, A.G. Marshall, Int. J. Mass Spectrom. 198 (2000) 113.
[6] D.M. Horn, R.A. Zubarev, F.W. McLafferty, J. Am. Soc. Mass Spectrom. 11 (1999) 320.
[7] J.E. Bruce, G.A. Anderson, M.D. Brand, L. Pasa-Tolic, R.D. Smith, J. Am. Soc. Mass Spectrom. 11 (2000) 416.
[8] M.E. Belov, E.N. Nikolaev, G.A. Anderson, K.J. Auberry, R. Harkewicz, R.D. Smith. J. Am. Soc. Mass Spectrom. 12 (2001) 38.
[9] M.E. Belov, M.V. Gorshkov, H.R. Udseth, G.A. Anderson, A.V. Tolmachev, D.C. Prior, R. Harkewicz, R.D. Smith, J. Am Soc. Mass Spectrom. 11 (2000) 19.
[10] E. Fischer. Z. Phys. 156 (1959) 26.
[11] E.P. Sheretov, V.A. Zenkin. V.F. Samorodov, Sov. Phys. Tech. Phys. 18 (1973) 282.
[12] C. Schwebel, P.A. Möller, P.T. Mahn, Rev. Phys. Appl. 10 (1975) 227.
[13] J.-C. Mathurin, S. Gregoire, A. Brunot, J.-C. Tabet, R.E. March, S. Catinella, P. Traldi, J. Mass Spectrom. 32 (1997) 829.
[14] J.F.J. Todd, R.M. Waldren, R.E. Mather, Int. J. Mass Spectrom. Ion Processes 34 (1980) 325.
[15] R.E. March, J. Mass Spectrom. 32 (1997) 351.
[16] J.M. Campbell, B.A. Collings, D.J. Douglas, Rapid Commun. Mass Spectrom. 12 (1998) 1463.
[17] K. Sannes-Lowery, R.H. Griffey, G.H. Kruppa, J.P. Speir, S.A. Hofstadler, Rapid Commun. Mass Spectrom. 12 (1998) 1957.
[18] D.H.E. Dubin, T.M. O'Neil, Rev. of Modern Phys. 71 (1999) 87.
[19] G.-Z. Li, J.A. Jarrell, Proceeding of the 46th ASMS Conference on Mass Spectrometry Allied Topics, Orlando, FL, June 1–6, 1998.
[20] A.V. Tolmachev, H.R. Udseth, R.D. Smith, Anal. Chem. 72 (2000) 970.
[21] A.J. Peurrung, R.T. Kouzes, S.E. Barlow, Int. J. Mass Spectrom. Ion Processes 157/158 (1996) 39.
[22] M.V. Gorshkov, L. Pasa Tolic, H.R. Udseth, G.A. Anderson, B.M. Huang, J.E. Bruce, D.C. Prior, S.A. Hofstadler, L. Tang, L.-Z. Chen, J.A. Willett, A.L. Rockwood, M.S. Sherman, R.D. Smith, J. Am. Soc. Mass Spectrom. 9 (1998) 692.
[23] M.E. Belov, M.V. Gorshkov, G.A. Anderson, H.R. Udseth, R.D. Smith, Anal. Chem. 72 (2000) 2271.
[24] D. Gerlich, Adv. Chem. Phys. 82 (1992), 1.
[25] H.G. Dehmelt, Adv. Atom. Mol. Phys. 3 (1967) 53.
[26] Quadrupole Mass Spectrometry and Its Applications, P.H. Dawson, (Ed.) North Holland, Amsterdam 1976
[27] A.V. Tolmachev, H.R. Udseth, R.D. Smith, Rapid Commun. Mass Spectrom. 14 (2000) 1907.
[28] A. Tolmachev, R. Harkewicz, K. Alving, C. Masselon, G. Anderson, V. Rakov, L. Pasa- Tolic, E. Nikolaev, M. Belov, H. Udseth, R. Smith, Proceeding of the 48th ASMS Conference on Mass Spectrometry, Long Beach, CA, 2000.
[29] R.E. March, R.J. Hughes, in Chemical Analysis, J.D. Winefordner (Ed.), Wiley, London 1991.
[30] K.L. Hunter, B.J. McIntosh, Int. J. Mass Spectrom. Ion Processes 87 (1989) 157.
[31] B.J. McIntosh, K.L. Hunter, Int. J. Mass Spectrom. Ion Processes 87 (1989) 165.
[32] K. Jungmann, J. Hoffnagle, R.G. DeVoe, R.G. Brewer, Phys. Rev. A 36 (1987) 345.
[33] E.A. Mason, E.W. McDaniel, Transport Properties of Ions in Gases, Wiley, New York 1988.